Chemical Engineering Journal 163 (2010) 108–118

Contents lists available at ScienceDirect

Chemical Engineering Journal

journal homepage: www.elsevier.com/locate/cej

Relationship between flow structure and mass transfer in fast fluidized bed

Baolin Hou[a,b], Hongzhong Li[a,*], Qingshan Zhu[a]

[a] State Key Laboratory of Multi-phase Complex Systems, Institute of Process Engineering, Chinese Academy of Sciences, P.O. Box 353, Beijing 100190, PR China
[b] Graduate School of Chinese Academy of science, Beijing 100049, PR China

ARTICLE INFO

Article history:
Received 26 April 2010
Received in revised form 7 July 2010
Accepted 12 July 2010

Keywords:
Fluidization
Multiphase flow
Multi-scale mass transfer
Particles
Structure

ABSTRACT

This paper analyzes the relationship between flow structure and mass transfer in fast fluidized beds for Geldart A and B particles. It does this by employing the eight heterogeneous local bed structural parameters (U_{fd}, U_{fc}, U_{pd}, U_{pc}, d_c, f, ε_d and ε_c) solved by Wang et al. [W. Wang, J. Li, Simulation of gas–solid two-phase flow by a multi-scale CFD approach of the EMMS model to the sub-grid level, Chemical Engineering Science, 62 (2007) 208–231] using the energy-minimization multi-scale (EMMS) model, in conjunction with a proposed theory on multi-scale mass transfer (MSMT) in a fast fluidized bed using the user defined scalars function in the commercial software Fluent 6.2.16 to solve the related mass conversion equations. The influence of the size and behavior of clusters on mass transfer in fast fluidized beds is discussed. The reaction in a fast fluidized bed is considered to comprise inside diffusion and outside diffusion of the particles as well as intrinsic reaction kinetics. Based on this theory and method, the decomposition of ozone at ambient temperature is calculated in a fast fluidized bed with average and local bed structure parameters and the axial and radial dimensionless concentrations of ozone and averaged mass transfer coefficients are compared to experimental data from the literature. The agreement between calculation and experimental data is good.

1. Introduction

Due to the high gas–solid contact area and good mass/heat transfer of the circulating fluidized bed (CFB), it has been used successfully in many industrial processes, e.g., combustion of low-grade fuels, mineral processing, and fluid catalytic cracking. However, because the complicated mechanism between the fluid dynamics and mass transfer is not clearly understood, the design and scale-up of CFBs is still not an easy task. The main reason is the existence of solid clusters and strands in the fast fluidized bed [1,2], leading to great difficulty in accurately predicting momentum, mass and heat transfer.

This work discusses the mass transfer aspect of CFB. Many researchers have employed empirical correlations and theoretical approaches to predict the dimensionless mass transfer number inside a fast fluidized bed, e.g., the following empirical correlation was proposed by Frossling [3] for dimensional analysis:

$$Sh = 2.0 + K(Re)^{1/n}(Sc)^{1/m} \quad (1)$$

Using the above equation, many authors [4,5] correlated their experimental data to obtain empirical values of the parameters K, n and m. Davidson and Basu [6,7] proposed that under a stagnant gas flow, a limiting value of 2 should be multiplied by the bed voidage, and La Nauze and Jung [8–11] proposed the following equation based on their experimental data:

$$Sh = 2\varepsilon + 0.69\left(\frac{U_s d_p \rho_f}{\varepsilon \mu_f}\right)^{1/2}(Sc)^{1/3} \quad (2)$$

Recently, Paterson and Hayhurst [12] provided further theoretical background for this expression. For mass transfer between a gas and solid in fluidized beds, many theoretical approaches have been proposed, for example, the steady-state boundary layer theory as first developed by Tamarin [13], and later improved by La Nauze [14,15] who proposed an unsteady-state model based on the frequency of gas renewal, leading to an improved matching of the model with experiment [15].

Breault [16] and Scala [17] found that the mass transfer coefficients differ by up to seven orders of magnitude in the literature; hence the need for a satisfactory model. The effects of bed structures on momentum transfer have also been studied [18–21]. Gao and Chang [22] and Berend and Srdjan [23] employed cluster size to replace particle diameter in formulating local drag force and granular temperature, with good results in predicting solid and

* Corresponding author. Tel.: +86 10 62556951; fax: +86 10 62536108.
E-mail address: hzli@home.ipe.ac.cn (H. Li).

1385-8947/$ – see front matter © 2010 Elsevier B.V. All rights reserved.
doi:10.1016/j.cej.2010.07.028

Nomenclature

a_p	specific surface area of particle (m^{-1})
a_c	specific surface area of cluster (m^{-1})
c_c	active component concentration of gas in cluster phase (kg/m^3)
c_d	active component concentration of gas in dispersed phase (kg/m^3)
c_f	averaged component concentration of gas (kg/m^3)
c_{sc}	active component concentration of gas near the surface of particle in cluster phase (kg/m^3)
c_{sd}	active component concentration of gas near the surface of particle in dispersed phase (kg/m^3)
c_{si}	active component concentration of gas near the surface of particle on the surface of cluster phase (kg/m^3)
c_{sf}	averaged active component concentration of gas near the surface of particles (kg/m^3)
C_{Dc}	drag coefficient in cluster phase
C_{Dd}	drag coefficient in dispersed phase
C_{Di}	drag coefficient between cluster and gas in dispersed phase
$\overline{C_D}$	averaged drag coefficient
D	gas diffusion coefficient (m^2/s)
d_c	diameter of cluster (m)
d_p	diameter of particle (m)
f	volume friction of cluster phase
K	coefficient of mass transfer between gas and particles swarm in homogeneous gas–particles system (m/s)
K_c	coefficient of mass transfer between gas and particles in cluster phase (m/s)
K_d	coefficient of mass transfer between gas and particles in dispersed phase (m/s)
K_f	coefficient of mass transfer (m/s)
$\overline{K_f}$	averaged coefficient of mass transfer (m/s)
K_i	coefficient of mass transfer between cluster and gas in dispersed phase (m/s)
k_r	the rate of reaction of ozone decomposition (s^{-1})
M	mass of naphthalene transferred from naphthalene particles to air flow in unit volume of the system ($kg/(m^3\ s)$)
M_a	mass transferred from particles to air due to aggregating and dispersing of the particles in unit volume of the system ($kg/(m^3\ s)$)
M_{ac}	mass transferred from particles in cluster phase to air in cluster phase in unit volume of the system ($kg/(m^3\ s)$)
M_{ad}	mass transferred from particles in dispersed phase to air in dispersed phase in unit volume of the system ($kg/(m^3\ s)$)
M_{dc}	mass transferred from high-concentration gas in the cluster/dispersed to the low-concentration gas in the dispersed/cluster phase by diffusion and seepage ($kg/(m^3\ s)$)
M_i	mass transferred from particles on the surface of clusters to air in dispersed phase in unit volume of the system ($kg/(m^3\ s)$)
M_{in}	the mass of active component entered the element slice (kg)
M_{out}	the mass of active component exited from the element slice (kg)
M_{ind}	the mass of active component entered the element slice in the dispersed phase (kg)
M_{outd}	the mass of active component exited from the element slice in the dispersed phase (kg)
Sc	Schmidt number
Sh	Sherwood number
t_{fc}	temperature of gas in cluster phase (K)
t_{fd}	temperature of gas in dispersed phase (K)
t_{pc}	temperature of particles in cluster phase (K)
t_{pd}	temperature of particles in dispersed phase (K)
U_f	superficial gas velocity (m/s)
U_{fc}	superficial gas velocity in cluster phase (m/s)
U_{fd}	superficial gas velocity in dispersed phase (m/s)
U_p	superficial particle velocity (m/s)
U_{pc}	superficial particle velocity in cluster phase (m/s)
U_{pd}	superficial particle velocity in dispersed phase (m/s)
U_s	superficial slip velocity between gas and particles
U_{sc}	superficial slip velocity between gas and particle in cluster phase (m/s)
U_{sd}	superficial slip velocity between gas and particle in dispersed phase (m/s)
U_{si}	superficial slip velocity gas between in dispersed phase and cluster (m/s)
W	mass flux of solid ($kg/(m^2\ s)$)

Greek letters

ε	voidage
ε_c	voidage in cluster phase
ε_d	voidage in dispersed phase
ε_f	averaged voidage
ε_i	voidage of inter-phase, i.e., the volume friction of gas except gas in clusters
μ_f	viscosity of gas ($kg/(m\ s)$)
ρ_f	density of gas (kg/m^3)
ρ_p	density of particle (kg/m^3)
η	the internal diffusion effectiveness factor of catalyst

species concentrations that were close to the experimental data. Cluster behaviors, aggregating and dispersing due to fluid–particle and particle–particle interactions, thus play an important role in both momentum and mass transfer [24–26].

Recently, Dong et al. [27,28] employed the multi-scale subgrid model developed by Wang and Li [19] and computational fluid dynamics (CFD) to investigate the influence of flow structure on local mass exchange between the dispersed and the cluster phases, and this showed good agreement with the experimental data. Gidaspow and co-workers [29,30] employed the diameter of clusters to replace the diameter of particles to study mass transfer on the basis of his granular kinetics theory. So, to characterize the general process of coupling mass transfer and reaction in a fast fluidized bed, the influence of bed structure on mass transfer is of paramount significance.

Our previous work [31] studied the relationships between bed structure and momentum, mass and heat transfer coefficients in a fast fluidized bed, but only limited to average parameters. In the present work, the energy-minimization multi-scale (EMMS) model [19,32] is employed to calculate the eight averaged and local bed structural parameters (U_{fd}, U_{fc}, U_{pd}, U_{pc}, d_c, f, ε_d and ε_c) in fast fluidized beds, the relationship between mass transfer and bed structure is analyzed, and a common theory on multi-scale mass transfer (MSMT) coupled with reaction in a fast fluidized bed is developed, with due consideration being given to inside diffusion, outside diffusion of particles and intrinsic kinetics. The coefficient of mass transfer is calculated on the basis of local and averaged bed structural parameters. The values from simulation for mass

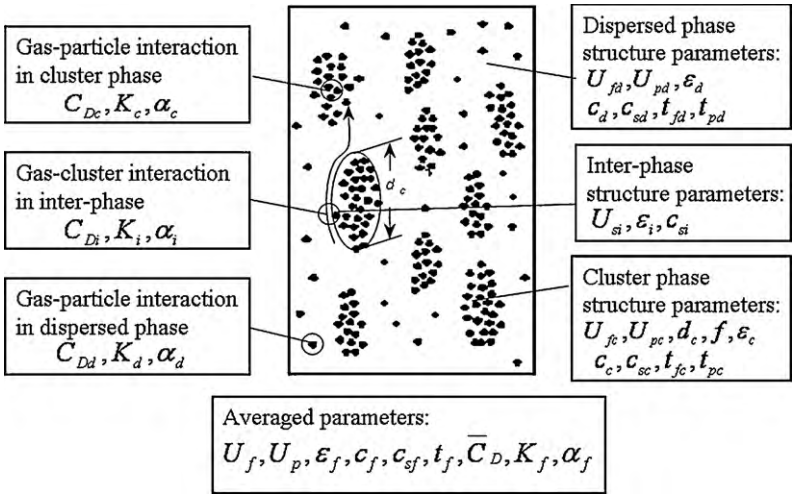

Fig. 1. Resolution of structure and gas–particles interaction in fast fluidized bed.

transfer based on the theory are compared with the experimental results reported by Subbarao and Gambhir [33] and Ouyang et al. [34].

2. Quantitative description of local structure and gas–particles interaction in fast fluidized bed

According to the EMMS model [32], which quantitatively describes the local bed structure of the fast fluidized bed, eight parameters are needed: voidages in the dispersed and the cluster phases ε_d, and ε_c respectively; superficial gas velocities in the dispersed and the cluster phases U_{fd}, and U_{fc} respectively; superficial particle velocities in the dispersed and the cluster phases U_{pd}, and U_{pc} respectively; diameter of cluster d_c; volume fraction of cluster phase f. The eight parameters of the local bed structure can be predicted by using the EMMS model when the superficial gas velocity U_f, superficial particle velocity U_p, gas density ρ_f, gas viscosity μ_f, particle density ρ_p, and particle diameter d_p are given, as was proposed by Li and Kwauk [32], and improved upon by other researchers [19,35].

The resolution of structure and gas–particles interaction in the fast fluidized bed is shown in Fig. 1, indicating that if mass and heat transfers are simulated, additional parameters are needed, viz., the component concentrations of gas in the dispersed phase and the cluster phase, c_d and c_c; the temperatures of gas in the dispersed phase and the cluster phase, t_{fd} and t_{fc}; the temperatures of particles in the dispersed phase and the cluster phase, t_{pd} and t_{pc}; the concentrations of active components near the surface of particles in the dispersed phase, in the cluster phase and on the surface of the cluster, c_{sd}, c_{sc} and c_{si} respectively. These parameters can be obtained by using the mass conservation equations and heat conservation equations for the dispersed phase and cluster phase respectively. The parameters for gas–particles interaction, i.e., drag coefficient C_D, mass transfer coefficient K_f and heat transfer coefficient α_f, are functions of the structure parameters.

3. Coefficient of mass transfer $\overline{K_f}$

3.1. Coefficient of mass transfer between gas and particles in homogeneous gas–particles system

In this case, the Yung–La Nauze [11] equation, Eq. (2), is recommended where Sh is the Sherwood number, Sc is the Schmidt number, and ε is voidage:

$$Sh = \frac{Kd_p}{D} \tag{3}$$

$$Sc = \frac{\mu_f}{\rho_f D} \tag{4}$$

In the above equations, D is the gas diffusion coefficient, and K is the coefficient of mass transfer. Substituting Eqs. (3) and (4) into Eq. (2) yields:

$$K = Sh\frac{D}{d_p} = 2\varepsilon\frac{D}{d_p} + 0.69\frac{D}{d_p}\left(\frac{U_s d_p \rho_f}{\varepsilon\mu_f}\right)^{1/2}\left(\frac{\mu_f}{\rho_f D}\right)^{1/3} \tag{5}$$

3.2. Coefficients of mass transfer between gas and particles in dispersed phase, in cluster phase, and interface for heterogeneous gas–particles system

Fig. 1 shows, analogous to Eq. (5), the interactions between gas and individually dispersed particles K_d, and particles inside clusters K_c, and particles outside the clusters K_i, respectively as

$$K_d = 2\varepsilon_d\frac{D}{d_p} + 0.69\frac{D}{d_p}\left(\frac{U_{sd} d_p \rho_f}{\varepsilon_d\mu_f}\right)^{1/2}\left(\frac{\mu_f}{\rho_f D}\right)^{1/3} \tag{6}$$

$$K_c = 2\varepsilon_c\frac{D}{d_p} + 0.69\frac{D}{d_p}\left(\frac{U_{sc} d_p \rho_f}{\varepsilon_c\mu_f}\right)^{1/2}\left(\frac{\mu_f}{\rho_f D}\right)^{1/3} \tag{7}$$

$$K_i = 2\varepsilon_d(1-f)\frac{D}{d_c} + 0.69\frac{D}{d_c}\left(\frac{U_{si} d_c \rho_f}{\varepsilon_d(1-f)\mu_f}\right)^{1/2}\left(\frac{\mu_f}{\rho_f D}\right)^{1/3} \tag{8}$$

where U_{sd} is the superficial slip velocity between the gas and individually dispersed particles:

$$U_{sd} = U_{fd} - U_{pd}\frac{\varepsilon_d}{1-\varepsilon_d} \tag{9}$$

U_{sc} is the superficial slip velocity between the gas and particles inside clusters:

$$U_{sc} = U_{fc} - U_{pc}\frac{\varepsilon_c}{1-\varepsilon_c} \tag{10}$$

and U_{si} is the superficial slip velocity between the gas and particles outside clusters:

$$U_{si} = \left(U_{fd} - U_{pc}\frac{\varepsilon_d}{1-\varepsilon_c}\right)(1-f) = \left(\frac{U_{fd}}{\varepsilon_d} - \frac{U_{pc}}{1-\varepsilon_c}\right)\varepsilon_d(1-f) \tag{11}$$

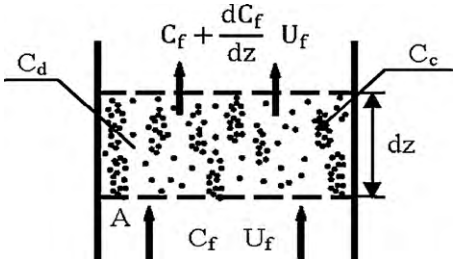

Fig. 2. Mass transfer between gas and particles in differential elemental slice.

3.3. Mass transfer between gas and particles in heterogeneous gas–particles system

Fig. 2 shows the mass transfer between the gas and particles in a horizontal differential elemental slice of a fast fluidized bed.

The mass M of active components transferred from the surface particles to gas phase in the elemental slice consists of four components: mass M_d transferred from individually dispersed particles to gas in the dispersed phase, mass M_c transferred from particles inside clusters to gas in the cluster phase, mass M_i transferred from particles on the surface of clusters to gas in the dispersed phase, and added mass M_a transferred from particles to gas due to aggregating and dispersing of the particles, expressed respectively as follows,

$$M_d = K_d a_p A dz(1-\varepsilon_d)(1-f)(c_{sd}-c_d) \tag{12}$$

$$\begin{aligned} M_c &= K_c A dz(a_p(1-\varepsilon_c)f - a_c(1-\varepsilon_c)f)(c_{sc}-c_c) \\ &= K_c A dz(a_p - a_c)(1-\varepsilon_c)f(c_{sc}-c_c) \end{aligned} \tag{13}$$

$$M_i = K_i a_c A dz(1-\varepsilon_c)f(c_{si}-c_d) \tag{14}$$

$$M_a = m_a A dz \tag{15}$$

where a_p is the specific surface area of the particle, $a_p = 6/d_p$ for a spherical particle; a_c is the specific surface area of the cluster, $a_c = 6/d_c$ for a spherical cluster; m_a is added mass transferred from particles to gas due to aggregating and dispersing of the particles in unit volume of the elemental slice.

It should be noted that when the interfacial area between the gas and particles in the cluster phase is calculated, the contact area between the particles on the surface of the cluster and gas in the dispersed phase should be subtracted as shown in Eq. (13).

Mass conservation calls for the following mass balance:

$$M = M_c + M_d + M_i + M_a \tag{16}$$

Substituting Eqs. (12)–(15) into Eq. (16) yields:

$$\begin{aligned} M = {} & (K_d a_p(1-\varepsilon_d)(1-f)(c_{sd}-c_d) + K_c(a_p-a_c)(1-\varepsilon_c)f(c_{sc}-c_c) \\ & + K_i a_c(1-\varepsilon_c)f(c_{si}-c_d))Adz + m_a A dz \end{aligned} \tag{17}$$

3.4. Averaged coefficient of mass transfer $\overline{K_f}$

The averaged coefficient of mass transfer is defined as

$$M = \overline{K_f} a_p A dz(1-\varepsilon_f)(c_{sf}-c_f) \tag{18}$$

where c_f and c_{sf} are the averaged concentrations of active components in the gas and on the surface of particles, and c_f is defined as

$$c_f \varepsilon_f = c_d \varepsilon_d (1-f) + c_c f \varepsilon_c \tag{19}$$

The equation for the averaged coefficient of mass transfer $\overline{K_f}$ can thus be given by comparing Eq. (17) with Eq. (18) as follows:

$$\overline{K_f} = \frac{K_d a_p(1-\varepsilon_d)(1-f)(c_{sd}-c_d) + K_c(a_p-a_c)(1-\varepsilon_c)f(c_{sc}-c_c) + K_i a_c(1-\varepsilon_c)f(c_{si}-c_d) + m_a}{a_p(1-\varepsilon_f)(c_{sf}-c_f)} \tag{20}$$

The traditional equation for the averaged coefficient of mass transfer as shown below:

$$\overline{K_f} = 2\varepsilon_f \frac{D}{d_p} + 0.69 \frac{D}{d_p} \left(\frac{U_s d_p \rho_f}{\varepsilon_f \mu_f} \right)^{1/2} \left(\frac{\mu_f}{\rho_f D} \right)^{1/3} \tag{21}$$

is however quite different from Eq. (20). The averaged coefficient of mass transfer $\overline{K_f}$ is affected by many parameters of the bed structure for the heterogeneous gas–particles flow system rather than by the average voidage ε_f and the superficial slip velocity U_s only.

4. Mass transfer equation for the dispersed phase and cluster phase

The purpose of developing mass transfer equations for the cluster phase and for the dispersed phase is to determine the concentrations of active component in the gas of the cluster phase and in the gas of the dispersed phase, c_c and c_d respectively. The mass of active components transferred from the surface of the particles to gas in the dispersed phase consists of four parts: mass M_d and mass M_i as mentioned above, mass M_{dc} transferred from high-concentration gas in the cluster to the low-concentration gas in the dispersed phase by diffusion and seepage, and M_{ad} transferred from particles to gas in the dispersed phase due to aggregating and dispersing of the particles.

According to the principle of mass transfer:

M_{dc} can be expressed by

$$M_{dc} = A dz K_{dc} a_c f \varepsilon_c (c_c - c_d) \tag{22}$$

where K_{dc} is the coefficient of mass exchange between lower concentration gas in the cluster phase and higher concentration gas in the dispersed phase, and, for spherical particles, can be expressed by the equation developed by Higbie [36]:

$$K_{dc} = 2.0 \frac{D\varepsilon_c}{d_c} + \sqrt{\frac{4D\varepsilon_c}{\pi t_1}} \tag{23}$$

where t_1 can be written as

$$t_1 = \frac{d_c}{\left| (U_{fc}/\varepsilon_c) - (U_{pc}/1-\varepsilon_c) \right|} \tag{24}$$

$$M_{ad} = m_{ad} A dz \tag{25}$$

The mass of active component M_{ind} entering the elemental slice should be

$$M_{ind} = U_{fd} A (1-f) c_d \tag{26}$$

The mass of active component M_{outd} exiting from the elemental slice should be

$$M_{outd} = U_{fd} A (1-f)(c_d + dc_d) \tag{27}$$

Thus the mass conservation equation for the active gas component in the dispersed phase can be expressed as

$$M_{outd} - M_{ind} = M_d + M_i + M_{dc} + M_{ad} \tag{28}$$

Substituting Eqs. (12), (14), (22), (25)–(27) into Eq. (28) yields:

$$\begin{aligned} U_{fd}(1-f)\frac{dc_d}{dz} = {} & K_d a_p(1-\varepsilon_d)(1-f)(c_{sd}-c_d) + K_i a_c(1-\varepsilon_c)f(c_{si}-c_d) \\ & + K_{dc} a_c f \varepsilon_c (c_c - c_d) + m_{ad} \end{aligned} \tag{29}$$

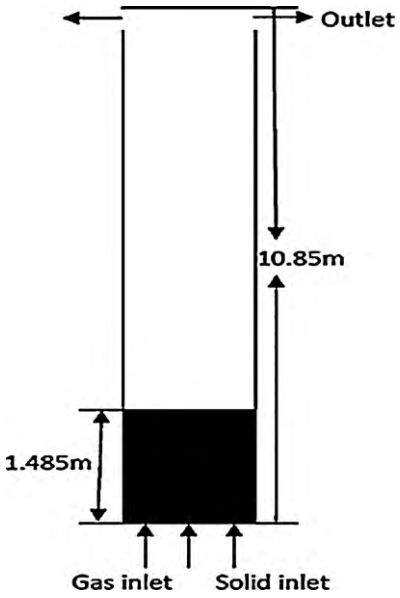

Fig. 3. The simulation domain.

Similarly, the mass conservation equation for the active gas component in the cluster phase can be derived as follows:

$$U_{fc}f\frac{dc_c}{dz}=K_c(a_p-a_c)(1-\varepsilon_c)f(c_{sc}-c_c)-K_{dc}a_cf\varepsilon_c(c_c-c_d)+m_{ac} \quad (30)$$

where m_{ac} is the added mass transferred from particles to gas in the cluster phase due to aggregating and dispersing of the particles in unit volume of the elemental slice.

However, under steady conditions, the dispersion of particles should equal their aggregation, thus counteracting each other. Therefore, M_a M_{ad} and M_{ac}, which represent the mass transferred from particles to gas due to aggregating and dispersing of the particles, could be neglected, as has been discussed in detail elsewhere [31].

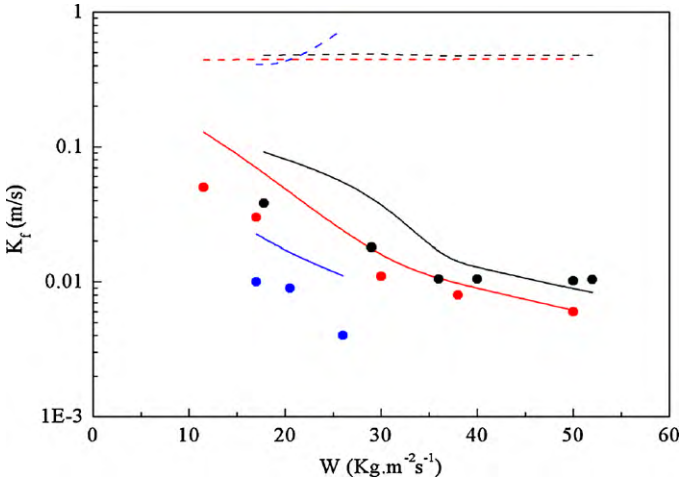

Fig. 4. Comparison of simulation with the Subbarao's and Gambhir's [33] experimental data (d_p = 395e−6m) and simulation (blue: u_f = 4 m/s; red: u_f = 5 m/s, black: u_f = 6 m/s; dot: experimental data; line: results of simulation by Eq. (20); dot line: results of simulation by Eq. (21)). (For interpretation of the references to colour in this figure legend, the reader is referred to the web version of the article.)

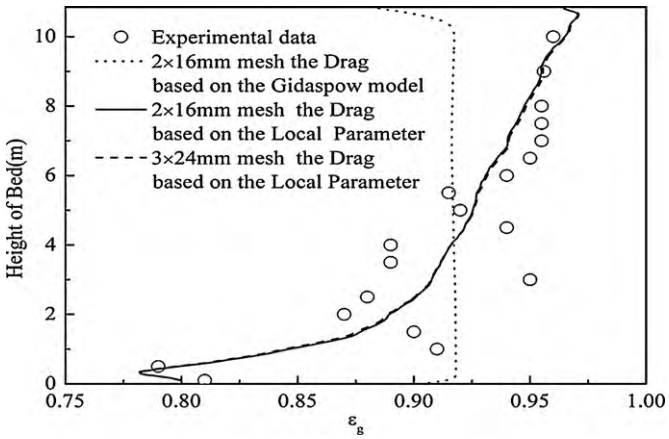

Fig. 5. Axial voidage distribution along the bed height.

5. Case study and calculation of mass transfer coefficient

5.1. Determination of boundary conditions

In this work, the averaged coefficient of mass transfer derived experimentally by Subbarao and Gambhir [33] will be calculated. Subbarao employed sand to adsorb naphthalene from saturated air in a fast fluidized bed to measure the mass transfer between gas and solid [33]. According to the conditions of the experiment, the process, in which the naphthalene in air is adsorbed by sand, is controlled by outside diffusion, and the desorption of naphthalene can be ignored; thus the naphthalene concentration on the surface of sand can be assumed to be zero, that is c_s = 0.0, c_{sc} = 0.0, c_{sd} = 0.0 and c_{si} = 0.0.

Since air is saturated with naphthalene upon entering the fluidized bed, the boundary can be written as:

$$c_c|_{z=0} = c^* \quad (31)$$

$$c_d\big|_{z=0} = c^* \quad (32)$$

where c^* is the naphthalene concentration at the saturated vapor pressure at a certain temperature.

For the given conditions, the heterogeneous flow structure (ε_c, ε_d, f, d_c, U_{sc}, U_{sd} and U_{si}) thus accords with the original EMMS model [32]. Mass conservation for naphthalene in the gas consists of Eqs. (29) and (30) and the boundary conditions of Eqs. (31) and (32). These are ordinary linear differential equations with given initial and boundary values, subject to standard solutions by Jenson and Jeffreys [37].

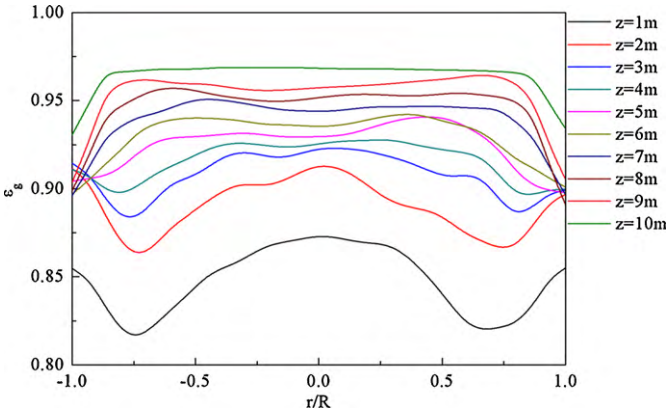

Fig. 6. Radial voidage distribution as function of bed height.

5.2. Determining concentration of active component near solid surface during reaction

In this paper, a first-order irreversible reaction is assumed to take place in a fast fluidized bed. In order to determine the concentration of active component near the solid surface, the equations for mass balance between reaction and mass transfer in the dispersed phase, in the cluster phase, in the inter-phase, and in the overall unit of reactor are given as follows.

For the dispersed phase,

$$k_r(1-\varepsilon_d)(1-f)c_{sd}\eta = K_d(1-\varepsilon_d)(1-f)a_p(c_d - c_{sd}) \tag{33}$$

For the cluster phase,

$$k_r\left((1-\varepsilon_c)f - 2(1-\varepsilon_c)f\frac{d_p}{d_c}\right)c_{sc}\eta = K_c((1-\varepsilon_c)fa_p - (1-\varepsilon_c)fa_c)(c_c - c_{sc}) \tag{34}$$

For the inter-phase,

$$2k_r(1-\varepsilon_c)f\frac{d_p}{d_c}c_{si}\eta = K_i(1-\varepsilon_c)fa_c(c_d - c_{si}) \tag{35}$$

For the overall unit volume of reactor,

$$k_r(1-\varepsilon_f)c_{sf}\eta = \overline{K_f}(1-\varepsilon_f)a_p(c_f - c_{sf}) \tag{36}$$

Based on the above equations, the equation for the averaged concentration on the surface of particles can be written as

$$(1-\varepsilon_f)c_{sf} = (1-\varepsilon_d)(1-f)c_{sd} + \left((1-\varepsilon_c)f - 2(1-\varepsilon_c)f\frac{d_p}{d_c}\right)c_{sc} + 2(1-\varepsilon_c)f\frac{d_p}{d_c}c_{si} \tag{37}$$

where η is the inter-diffusion effectiveness factor and k_r is the reaction rate constant for unit volume of catalyst particles.

In the above five equations only four equations are independent. Theoretically, only four among the five equations (33)–(37) need to be solved together with Eqs. (29) and (30) in order to determine the values of c_d, c_d, c_{sc}, c_{sd}, c_{si}, c_f. However, if the appropriate equations are not chosen, the numerical calculation might not converge. In general, if reaction takes place mainly in the dense phase, Eqs. (33), (35)–(37) will be chosen; otherwise Eqs. (33), (34), (35), and (37).

5.3. Mass transfer model based on bed structure coupled with CFD model

Unlike the conventional CFD model, which assumes uniform active concentrations in each calculating grid, in the MSMT model the active concentration in each grid can be divided into two parts: the active concentration in the dispersed phase c_d and that in the dense phase c_c. Thus, the active component is transported through convection, diffusion and exchange between the dense phase and the dispersed phase in each grid, and their respective mass conservation can be written as follows.

In the dispersed phase:

$$\frac{\partial((1-f)\varepsilon_d\rho_g X_d)}{\partial t} + \nabla((1-f)\varepsilon_d\rho_g X_d U_{fd} - (1-f)\varepsilon_d\rho_g D_{mi}\nabla X_d) - S_d = 0.0 \tag{38}$$

In the dense phase:

$$\frac{\partial(f\varepsilon_c\rho_g X_c)}{\partial t} + \nabla(f\varepsilon_c\rho_g X_c U_{fc} - f\varepsilon_c\rho_g D_{mi}\nabla X_c) - S_c = 0.0 \tag{39}$$

where X_d and X_c, defined as the mass fractions of the active component in the dispersed phase and the dense phase, can be calculated by the following equations:

$$X_d = \frac{c_d}{\rho_g} \tag{40}$$

$$X_c = \frac{c_c}{\rho_g} \tag{41}$$

Based on Eqs. (29) and (30), S_d and S_c can be calculated as follows:

$$S_d = K_d a_p(1-\varepsilon_d)(1-f)\left(\frac{K_d a_p}{k_r\eta + K_d a_p} - 1\right)\cdot X_d + K_i a_c(1-\varepsilon_c)f\left(\frac{K_i a_c}{2k_r\eta(d_p/d_c) + K_d a_c} - 1\right)\cdot X_d + K_{dc}a_c f\varepsilon_c(X_c - X_d) \tag{42}$$

$$S_c = K_c(a_p - a_c)(1-\varepsilon_c)f\left(\frac{K_c(a_p - a_c)}{k_r(1-2(d_p/d_c)) + K_d(a_p - a_c)} - 1\right)X_c - K_{dc}a_c f\varepsilon_c(X_c - X_d) \tag{43}$$

5.4. Solving Eqs. (29), (30), and Eqs. (38), (39)

Eqs. (29) and (30) are typical ordinary equations with known initial values, which can be solved by a numerical method, e.g., Runge-Kutta, calling for only local averaged flow structure parameters from the EMMS version developed by Li and Kwauk [32]. However, Eqs. (38) and (39) are partial differential equations, and uniform flow structure parameters are required for solving these equations, for which local averaged fluid information needs to be first provided by the two-fluid model (TFM) using Fluent 6.2.16, and then the local averaged flow structure parameter can be obtained from local averaged flow information in each calculation grid by EMMS [19]. Thus, Eqs. (38) and (39) can be solved by the user defined scalars (UDS) provided by Fluent 6.2.16, as described in detail in Appendix A. And the geometrical structure of the fast fluidized bed employed in calculating is described in detail in Fig. 3.

6. Result and discussion

In this work, the averaged coefficient of mass transfer of the whole bed has been calculated, and the results of the simulation are compared with the experimental data reported by Subbarao and Gambhir [33]. Fig. 4 shows that the simulation based on the current theory better approaches the experimental data than that of the traditional method of Eq. (21).

However, in order to further test and verify the theory for the case affected by both mass transfer and reactions in a fast fluidized bed, the process of ozone decomposition performed by Ouyang et al. [34] is simulated. The FCC particles are fluidized by air, and the ozone concentrations are measured axially and radially. Before calculating mass transfer in the fluidized bed, the fluid hydrodynamic is first simulated and compared with the experimental data as shown in Figs. 5 and 6. This indicates that the S-shape voidage profile axially and the low solids concentration at the center but high density near wall radially can be captured based on the drag model in this work, with good agreement being shown experiment and simulation. In Fig. 7, the average parameter means the averaged heterogeneous structure parameters for whole fast fluidized bed given by the first version of EMMS model developed by Li and Kwauk [32], which assumes that the heterogeneous structure parameters are same in the whole fast fluidized bed. The local

Table 1
Governing equations for two-fluid model and its constitutive relations.

Continuity equation ($k = g,s$)

$$\frac{\partial(\varepsilon_k\rho_k)}{\partial t} + \nabla(\varepsilon_k\rho_k u_k) = 0$$

$$\varepsilon_s + \varepsilon_g = 1$$

Momentum equation ($k = g, s$; $l = s, g$)

$$\frac{\partial(\varepsilon_k\rho_k u_k)}{\partial t} + \nabla(\varepsilon_k\rho_k u_k u_k) = -\varepsilon_k\nabla p_g + \varepsilon_k\rho_k g + \nabla\tau_k + \beta(u_l - u_k)$$

Species conversion equation for TFM

$$\frac{\partial(\varepsilon_g\rho_g X_i)}{\partial t} + \nabla(\varepsilon_g\rho_g u_g X_i) = -\varepsilon_g\rho_g D_i\nabla X_i + R_i$$

Species conversion equation for MSMT

Eqs. (38) and (39)

Gas phase stress

$$\tau_g = 2\mu_g S_g$$

Solid phase stress

$$\tau_s = [-p_s + \lambda_s\nabla\mu_s]\delta + 2\mu_s S_s$$

Deformation rate

$$S_k = \tfrac{1}{2}[\nabla u_k + (\nabla u_k)^T] - \tfrac{1}{3}\nabla u_k\delta$$

Solid phase pressure

$$p_s = \varepsilon_s\rho_s\Theta[1 + 2(1+e)\varepsilon_s g_0]$$

Solid phase shear viscosity

$$\mu_s = \tfrac{4}{3}\varepsilon_s^2\rho_s d_p g_0(1+e)\sqrt{\frac{\Theta}{\pi}} + \frac{2\mu_{s,dilute}}{(1+e)g_0}\left[1 + \tfrac{4}{5}(1+e)\varepsilon_s g_0\right]^2$$

$$\mu_{s,dilute} = \tfrac{5}{96}\rho_s d_p\sqrt{\pi\Theta}$$

Solid phase bulk viscosity

$$\lambda_s = \tfrac{4}{3}\varepsilon_s^2\rho_s d_p g_0(1+e)\sqrt{\frac{\Theta}{\pi}}$$

Radial distribution functions

$$g_0 = \left[1 - \left(\frac{\varepsilon_g}{\varepsilon_{sm}}\right)^{1/3}\right]^{-1}$$

Granular temperature equation

$$\tfrac{3}{2}\left[\frac{\partial(\varepsilon_s\rho_s\Theta)}{\partial t} + \nabla(\varepsilon_s\rho_s u_s\Theta)\right] = \tau_s : \nabla u_s - \nabla q - \gamma + \beta\overline{C_g C} - 3\beta\Theta$$

Collisional energy dissipation

$$\gamma = 3(1-e^2)\varepsilon_s^2\rho_s g_0\Theta\left[\frac{4}{d_p}\sqrt{\frac{\Theta}{\pi}} - \nabla u_s\right]$$

Flux of fluctuating energy

$$q = -k\nabla\Theta$$

Conductivity if the fluctuating energy

$$k = \frac{2k^k[1+(6/5)(1+e)\varepsilon_s g_0]^2}{(1+e)g_0} + k^c$$

$$k^k = \tfrac{75}{384}d_p\rho_s\sqrt{\Theta\pi}$$

$$k^c = 2\varepsilon_s^2\rho_s d_p g_0(1+e)\sqrt{\frac{\Theta}{\pi}}$$

Drag coefficient

Gidaspow (Gidaspow and Bezburuah, 1992)

$\varepsilon_g \geq 0.8$:

$$\beta = \tfrac{3}{4}C_D\frac{\varepsilon_s\varepsilon_g\rho_g|u_g - u_s|}{d_p}\varepsilon_g^{-2.65}$$

$\varepsilon_g < 0.8$

$$\beta = 150\frac{\varepsilon_g\varepsilon_s\mu_g}{\varepsilon_g d_p^2} + 1.75\frac{\rho_g\varepsilon_s|u_g - u_s|}{d_p}$$

In this work

$$\beta_0 = \frac{\varepsilon_g^2}{|u_g - u_s|}F_d$$

structure parameters means the heterogeneous structure parameter in every calculating grid, this can be gotten the model developed by Wang and Li [19]. Fig. 7 compares experimental data with calculation results for the longitudinal ozone concentration distribution, indicating fast ozone decomposition at the bottom of the bed. This is mainly attributed to the high starting ozone concentration and the S-shaped voidage profile in the fast fluidized bed. With increasing bed height, the rate of ozone decomposition decreases rapidly, until near the exit of the bed, it changes only slightly. Fig. 7 further shows that the present simulation theory approaches the experimental data more closely than the TFM and the plug-flow models. Fig. 8 compares the simulation results against experimental data for radial distribution of ozone concentration at different bed heights, indicating that except for the bottom of the fluidized bed, agreement is good. The difference at the bottom of the fluidized bed might be attributed to the difficulty of close measurement, as has been reported in the literature [34].

Dong et al. [28] also simulated the above cases, finding good agreement with the experimental data, without, however, considering the effect of the local structure on mass transfer, and employing the reaction rate constant including the influence of outside diffusion. But for most industrial processes, the rate of outside diffusion should be considered a function of slip velocity between gas and solid. The compromise between inside diffusion, outside diffusion, and intrinsic kinetics in the process of reaction, needs to be considered as a whole. However, at an ambient temperature the ozone decomposition reaction is mainly controlled by the intrinsic kinetics in each phase, so that the predicted result by

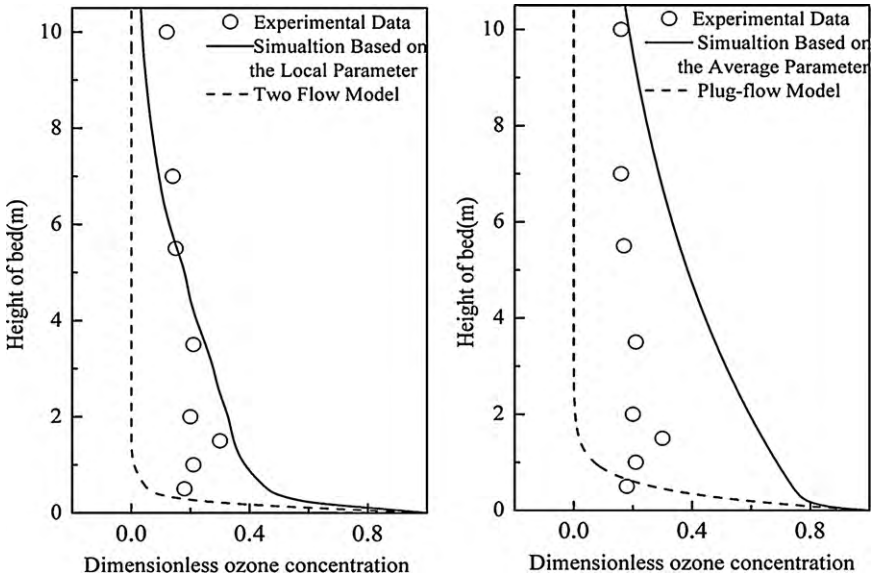

Fig. 7. Vertical ozone concentration distribution: comparison of simulation with Ouyang et al. [34] experimental data.

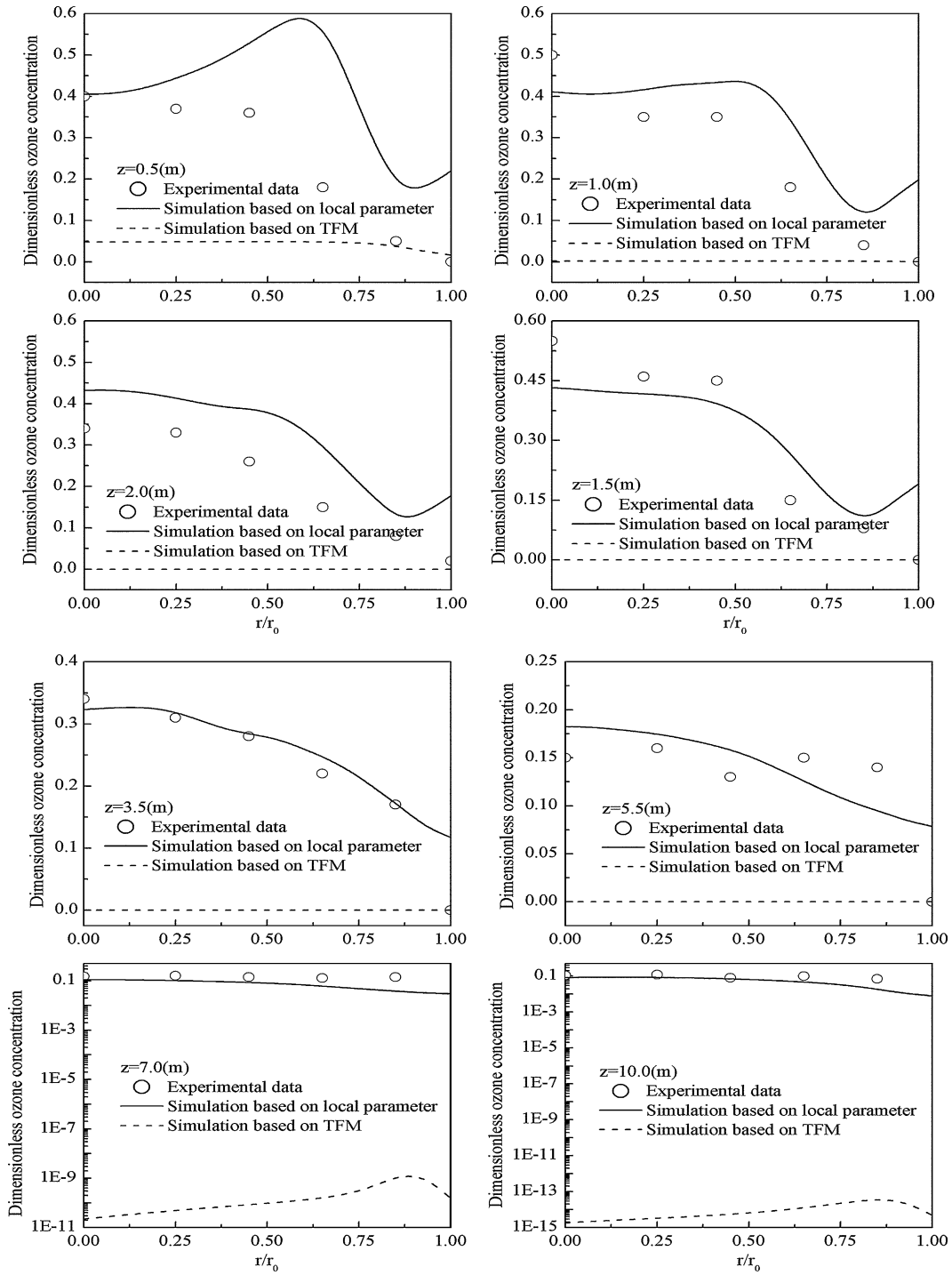

Fig. 8. (1) Radial ozone concentration distribution: comparison of simulation with Ouyang et al. [34] experimental data. (2) Radial ozone concentration distribution: comparison of simulation with Ouyang et al. [34] experimental data.

Dong et al. [28] is still in good agreement with the experimental data.

Fig. 9 shows the simulated ozone concentrations in the gas and on the surface of particles of dispersed phase, cluster phase, and the inter-phase, based on the averaged flow structure parameters under the operating conditions in Fig. 7. From Fig. 9, it can be seen that in the gas of the cluster phase the ozone concentration quickly decreases to almost zero at the bottom of reactor and is kept very low throughout the whole reactor. However, the ozone concentration in the gas of the dispersed phase changed slowly and is higher than in the cluster phase. This kind of phenomenon can be attributed to the heterogeneous structure in the fast fluidized bed; in other words, the catalyst is mainly included in the cluster phase. So that the reaction mainly happens in the cluster phase, the reaction of ozone decomposition in this circulating fluidized bed is controlled by the mass exchange of gas between the dispersed phase and the cluster phase.

Fig. 10 shows the differences between the ozone concentration on the surface of particles and the ozone concentration in the gas in the dispersed phase, cluster phase, and inter-phase at the same operating conditions as in Fig. 9. It can be seen from Fig. 10 that, although the ozone decomposition reaction has been known to be

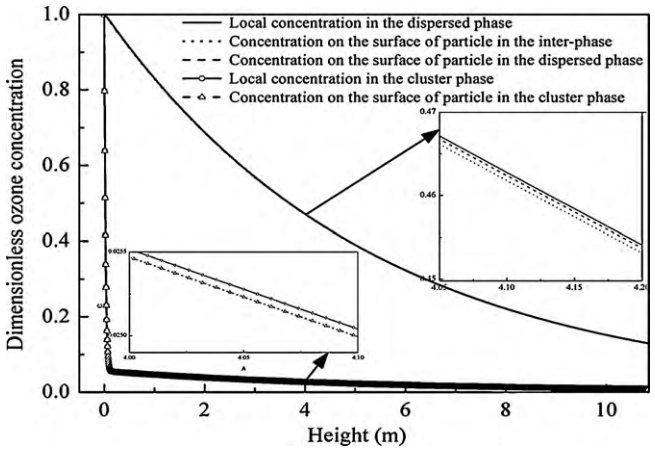

Fig. 9. Comparison of ozone concentration in gas of dispersed phase and cluster phase with that on the surface of particle in the dispersed phase, cluster phase, and in the inter-phase.

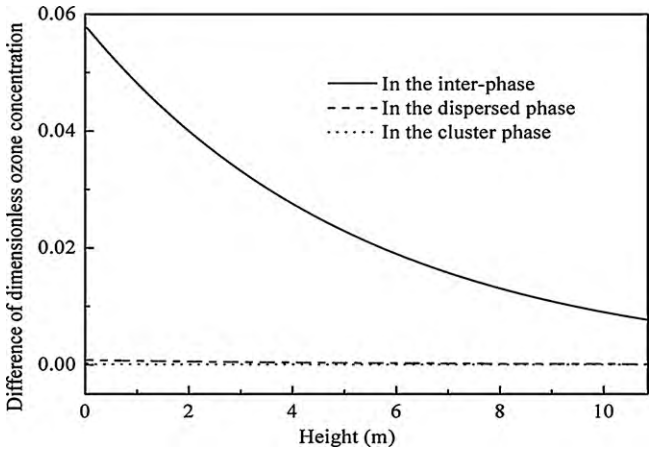

Fig. 10. Difference of the ozone concentrations between in the main gas and on the surface of particle in dispersed phase, in cluster phase and in the inter-phase respectively.

mainly controlled by the intrinsic kinetics in every phase, there are still the concentration differences between the gas and on the surface of particles in the dispersed phase, in the cluster phase and in the inter-phase. This implies that the reaction of ozone decomposition in every phase is slightly influenced by the outer diffusion. This phenomenon has also been described by Gidaspow and co-workers [29,30].

Table 2
Parameters setting for the simulation.

Particle diameter	65 μm
Particle density	1380 kg/m^3
Grid size, Δx	2 mm
Grid size, Δy	16 mm
Riser height	10.85 m
Superficial gas velocity, U_{g0}	3.8
Solids flux, G_s	106
Initial bed height, H_0	1.25
Coefficient of restitution	0.93
Time step	2.5e−4s
Unsteady formulation	First-order implicit
Pressure–velocity coupling	Phase coupled SIMPLE
Momentum discretization	First-order upwind
Maximum number of iterations per time step	30
Convergence criteria	1.0e−3
Maximum solid packing volume fraction	0.63

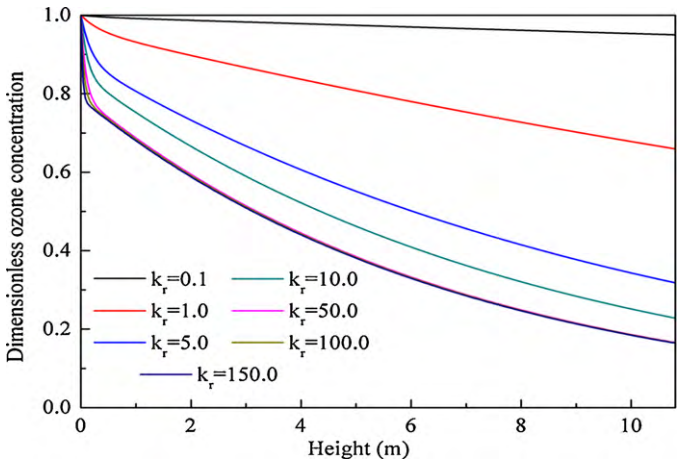

Fig. 11. Relation between ozone concentration profile and reaction rate constant.

The dimensionless ozone concentration as a function of the rate of the intrinsic reaction, which is simulated on the basis of averaged flow structure parameters, is shown in Fig. 11. It can be seen that when the intrinsic rate is less than 10, increasing the intrinsic rate will lead to a major increase in the ozone conversion along with the bed height; this means the reaction in the reactor is controlled by the intrinsic kinetics. However, when the intrinsic rate reaches 50, with the increase in the chemical intrinsic rate, the ozone concentration profile will not be changed in the whole reactor except at the bottom of the bed, which means the controlling step shifts from the chemical intrinsic rate to the mass exchange between the dispersed phase and cluster phase.

In Fig. 12, the dimensionless ozone concentration as a function of the diameter of cluster, which is simulated with the intrinsic reaction rate 57.2 and other conditions from the literature [34], is shown. From this figure, it can be seen that with a decrease in the diameter of the cluster, the conversion of ozone is greatly improved. But when the diameter of the cluster reaches a certain small value, the ozone conversion closely approaches the results of the plug-flow model. This means the controlling step shifts from the mass exchange between the dispersed phase and the dense phase to the chemical reaction intrinsic rate for ozone decomposition at the normal temperature, and the influence of cluster on mass transfer disappears.

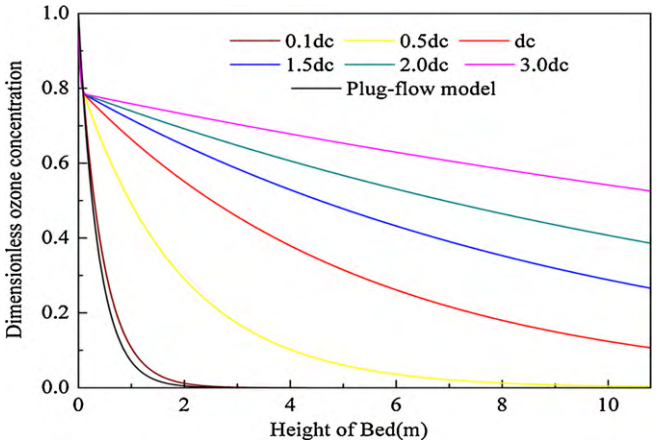

Fig. 12. Relation between ozone concentration profile and diameter of cluster (*dc* represents the diameter of cluster got from EMMS based on the experimental condition reported by Ouyang et al. [34]).

7. Conclusion

Based on the above discussion and comparison, it was found that there are the heterogeneous gas–particles flow structure has significant effects on the mass transfer process and mass transfer coefficient in fast fluidized beds. By comparing the simulation and experimental data for ozone decomposition in a fast fluidized bed, the results suggest the theory of MSMT, based on the local bed structural parameter, can better characterize the natural properties of the process of coupled mass and reaction in the fast fluidized bed than other traditional methods. In addition, the compromises between inside diffusion, outside diffusion, and intrinsic kinetics is considered in the MSMT model, which provides a common method to deal with the process of coupled mass and reaction in a fast fluidized bed. And using the MSMT, the active component concentrations in the gas and on the surface of the particles in the dispersed phase, in the cluster phase, and in the inter-phase can be calculated; thus the controlling step in every phase and throughout the whole reactor can be disclosed, providing the theoretical basis for designing and operating a highly efficient fast fluidized bed reactor. To sum up, the MSMT model in this paper can provide more accurate information about mass transfer and reaction in fast fluidized beds than other traditional methods, and it is expected that the MSMT model will be used to successfully scale-up and design fast fluidized beds in the future.

Acknowledgements

The author is grateful for the support for this work from the National Natural Science Foundation of China under Grant No. 20736004, and from the State Key Development Program for Basic Research of China (973 Program) under Grant No. 2007CB613502.

Appendix A. Appendix A

In this work, Gambit_2.2 was employed to generate the computational grid and Fluent 6.2.16 was used as the solver. In the calculation process, at first, the bed structure parameters can be solved by EMMS [19], based on the averaged voidage and the velocity of gas and solid from CFD. Thus the drag in Table 1 can be obtained, and Eqs. (38) and (39) can be solved by the function of UDS in the Fluent 6.2.16.

In the fluidized bed, the solid phase is often treated as fluid phase. Therefore, the Eulerian model can be used to model gas–solid fluidized bed reactors. And the granular kinetic theory is employed to calculate the viscous forces and the solid pressure of the particulate phase. The governing equations in Eulerian notation are given in Table 1.

The differential equations in Table 1 can be solved by a finite volume method. These equations are discretized by the first-order upwind differencing scheme over the used finite volume. The popular SIMPLE algorithm by Patankar [38] is used to solve the pressure from the gas phase momentum equation. Each simulation is performed for up to 25 s of real-time.

The inlet at the bed bottom is designated as the velocity inlet boundary condition for both the gas and solid phases. The boundary condition at the top of the bed is a pressure boundary fixed at atmospheric pressure. Solids are leaved from the top due to drag force and then return to the computational domain from the bottom inlet with the same mass flux. Other boundary conditions are specified as the wall, which are all set as no-slip wall boundary conditions for both the gas and solid phases. The parameters of the simulations are described in Table 2.

In Table 1, the drag in the calculating grid can be written as:

$$F_D = \frac{(1-\varepsilon_f)}{(\pi/6){d_p}^3}\overline{C_D}\frac{1}{2}\rho_f \left|U_s\right| U_s \frac{\pi}{4}{d_p}^2 \tag{A-1}$$

The equation for the averaged drag coefficient $\overline{C_D}$ can be expressed as

$$\overline{C_D} = \frac{\begin{array}{l} f(1-\varepsilon_c)(1-2(d_p/d_c))C_{Dc}\left|U_{sc}\right| U_{sc} \\ +(1-f)(1-\varepsilon_d)C_{Dd}\left|U_{sd}\right| U_{sd} + f(d_p/d_c)C_{Di}\left|U_{si}\right| U_{si} \end{array}}{(1-\varepsilon_f)\left|U_s\right| U_s} \tag{A-2}$$

where C_{Di} is the coefficient of drag between two phases, C_{Dc} is the coefficient of drag in the cluster, C_{Dd} is the coefficient of drag in the dispersed phase. The above equations for the drag in the calculating grid have been described in detail in the literature [36].

References

[1] O. Bolland, R. Nicolai, Describing mass transfer in circulating fluidized beds by ozone decomposition, Chemical Engineering Communications 187 (2001) 1–21.
[2] R.W. Breault, C.P. Guenther, Mass transfer in the core-annular and fast fluidization flow regimes of a CFB, Powder Technology 190 (2009) 385–389.
[3] N. Frossling, The evaporation of falling drops, Gerlands Beitrge zur Geophysik 52 (1938) 170–216.
[4] W.E. Ranz, J.R. Marshall, Evaporation from drops, Chemical Engineering Progress 48 (1952) 141–146.
[5] P.N. Rowe, K.T. Claxton, J.B. Lewis, Heat and mass transfer from a single sphere in an extensive flowing fluid, Transactions of the Institution of Chemical Engineers 43 (1965) T14–T31.
[6] J.F. Davidson, D. Harrison, Fluidized Particles, Cambridge University Press, Cambridge, 1963.
[7] P. Basu, J. Broughton, D.E. Elliott, Combustion of single coal particles in fluidized beds, in: Institute of Fuel Symposium Series No. 1. Fluidized Combustion, 1975, London, pp. A3-1–A3-10.
[8] R.D. La Nauze, K. Jung, The kinetics of combustion of petroleum coke particles in a fluidized-bed combustor, Proceedings of the Combustion Institute 19 (1982) 1087–1092.
[9] R.D. La Nauze, K. Jung, Combustion kinetics in fluidized beds, in: Proceedings of the Seventh International Conference on Fluidized Bed Combustion ASME, 1983, pp. 1040–1053.
[10] R.D. La Nauze, K. Jung, Mass transfer of oxygen to a burning particle in a fluidized bed, in: Proceedings of the Eighth Australasian Fluid Mechanics Conference, Newcastle, 1983, pp. 5C.1–C.15.
[11] K. Jung, R.D. La Nauze, Sherwood numbers for burning particles in fluidized beds, in: D. Kunii, S.S. Cole (Eds.), Fluidization IV Engineering Foundation, 1983, pp. 427–434.
[12] W.R. Paterson, A.N. Hayhurst, Mass or heat transfer from a sphere to a flowing fluid, Chemical Engineering Science 55 (2000) 1925–1927.
[13] A.I. Tamarin, Mass transfer between the gas and solid particles in a fluidized bed, Journal of Engineering Physics 41 (1982) 1346–1350.
[14] R.D. La Nauze, Fundamentals of coal combustion in fluidised beds, Chemical Engineering Research and Design 63 (1985) 3–33.
[15] R.D. La Nauze, K. Jung, Mass transfer relationships in fluidized-bed combustors, Chemical Engineering Communications 43 (1986) 275–286.
[16] R.W. Breault, A review of gas–solid dispersion and mass transfer coefficient correlations in circulating fluidized beds, Powder Technology 163 (2006) 9–17.
[17] F. Scala, Mass transfer around freely moving active particles in the dense phase of a gas fluidized bed of inert particles, Chemical Engineering Science 62 (2007) 4159–4176.
[18] J. Wang, W. Ge, J. Li, Eulerian simulation of heterogeneous gas–solid flows in CFB risers: EMMS-based sub-grid scale model with a revised cluster description, Chemical Engineering Science 63 (2008) 1553–1571.
[19] W. Wang, J. Li, Simulation of gas–solid two-phase flow by a multi-scale CFD approach of the EMMS model to the sub-grid level, Chemical Engineering Science 62 (2007) 208–231.
[20] N. Yang, W. Wang, W. Ge, L. Wang, J. Li, Simulation of heterogeneous structure in a circulating fluidized-bed riser by combining the two-fluid model with the EMMS approach, Industrial & Engineering Chemistry Research 43 (2004) 5548–5561.
[21] J. Gao, J. Chang, C. Xu, Y. Yang, CFD simulation of gas solid flow in FCC strippers, Chemical Engineering Science 63 (2008) 1827–1841.
[22] J. Gao, J. Chang, CFD modeling of mass transfer and stripping efficiency in FCCU strippers, AIChE Journal 54 (2008) 1164–1177.
[23] V.W. Berend, S. Srdjan, Derivation, simulation and validation of a cohesive particle flow CFD model, AIChE Journal 54 (2008) 9–19.
[24] Y.P. Tsuo, D. Gidaspow, Computation of flow patterns in circulating fluidized beds, AIChE Journal 36 (1990) 885–896.
[25] M. Tartan, D. Gidaspow, Measurement of granular temperature and stresses in risers, AIChE Journal 50 (2004) 1760–1775.

[26] J. Jung, D. Gidaspow, I.K. Gamwo, Measurement of two kinds of granular temperatures, stresses, and dispersion in bubbling beds, Industrial and Engineering Chemistry Research 44 (2005) 1329–1341.
[27] W. Dong, W. Wang, J. Li, A multiscale mass transfer model for gas–solid riser flows. Part II Sub-grid simulation of ozone decomposition, Chemical Engineering Science 63 (2008) 2811–2823.
[28] W. Dong, W. Wang, J. Li, A multiscale mass transfer model for gas–solid riser flows. Part 1. Sub-grid model and simple tests, Chemical Engineering Science 63 (2008) 2798–27810.
[29] B. Chalermsinsuwan, P. Piumsomboon, D. Gidaspow, Kinetic theory based computation of PSRI riser. Part II. Computation of mass transfer coefficient with chemical reaction, Chemical Engineering Science 64 (2009) 1212–1222.
[30] B. Chalermsinsuwan, P. Piumsomboon, D. Gidaspow, Kinetic theory based computation of PSRI riser. Part I. Estimate of mass transfer coefficient, Chemical Engineering Science 64 (2009) 1195–1211.
[31] B. Hou, H. Li, Relationship between flow structure and transfer coefficients in fast fluidized beds, Chemical Engineering Journal 157 (2010) 509–519.
[32] J. Li, M. Kwauk, Particle-fluid Two-phase Flow: The Energy-minimization Multiscale Method, Metallurgical Industry Press, BeiJing, 1994, pp. 23–40.
[33] D. Subbarao, S. Gambhir, Gas particle mass transfer in risers, in: J.R. Grace, J.X. Zhu, H. de Lasa (Eds.), Proceeding of the 7th International Conference on Circulating Fluidized Beds, Canadian Society for Chemical Engineering, Ottawa, Canada, 2002, pp. 97–104.
[34] S. Ouyang, X.G. Li, O.E. Potter, Circulating fluidized bed as a catalytic reactor: experimental study, AIChE Journal 41 (1995) 1534–1542.
[35] N. Yang, W. Wang, W. Ge, J. Li, CFD simulation of concurrent-up gas–solid flow in circulating fluidized beds with structure-dependent drag coefficient, Chemical Engineering Journal 96 (2003) 71–80.
[36] R. Higbie, The rate of absorption of a pure gas into a still liquid during short period of exposure, Trans Am hast Chem Eng 31 (1935) 365–389.
[37] V.G. Jenson, G.V. Jeffreys, Mathematical Methods in Chemical Engineering, Academic Press, 1977.
[38] S.V. Patankar, Numerical Heat Transfer and Fluid Flow, Hemisphere Publishing Corp., 1980.